Smart Structures and Systems, *Vol. 25, No. 1 (2020) 65-80*
DOI: https://doi.org/10.12989/sss.2020.25.1.065

Semi-active eddy current pendulum tuned mass damper with variable frequency and damping

Liangkun Wang [1,2a], Weixing Shi [1,2b], Ying Zhou*[1,2] and Quanwu Zhang [1,2c]

[1] *Department of Disaster Mitigation for Structures, Tongji University, Shanghai, 200092, P.R. China*
[2] *State Key Laboratory for Disaster Reduction of Civil Engineering, Tongji University, Shanghai, 200092, P.R. China*

(*Received November 22, 2018, Revised May 23, 2019, Accepted August 29, 2019*)

Abstract. In order to protect a structure over its full life cycle, a novel tuned mass damper (TMD), the so-called semi-active eddy current pendulum tuned mass damper (SAEC-PTMD), which can retune its frequency and damping ratio in real-time, is proposed in this study. The structural instantaneous frequency is identified through a Hilbert-Huang transformation (HHT), and the SAEC-PTMD pendulum is adjusted through an HHT-based control algorithm. The eddy current damping parameters are discussed, and the relationship between effective damping coefficients and air gaps is fitted through a polynomial function. The semi-active eddy current damping can be adjusted in real-time by adjusting the air gap based on the linear-quadratic-Gaussian (LQG)-based control algorithm. To verify the vibration control effect of the SAEC-PTMD, an idealized linear primary structure equipped with an SAEC-PTMD excited by harmonic excitations and near-fault pulse-like earthquake excitations is proposed as one of the two case studies. Under strong earthquakes, structures may go into the nonlinear state, while the Bouc-Wen model has a wild application in simulating the hysteretic characteristic. Therefore, in the other case study, a nonlinear primary structure based on the Bouc-Wen model is proposed. An optimal passive TMD is used for comparison and the detuning effect, which results from the cumulative damage to primary structures, is considered. The maximum and root-mean-square (RMS) values of structural acceleration and displacement time history response, structural acceleration, and displacement response spectra are used as evaluation indices. Power analyses for one earthquake excitation are presented as an example to further study the energy dissipation effect of an SAEC-PTMD. The results indicate that an SAEC-PTMD performs better than an optimized passive TMD, both before and after damage occurs to the primary structure.

Keywords: tuned mass damper; semi-active control; variable pendulum; eddy current damping; variable damping; nonlinear control

1. Introduction

Tuned mass dampers (TMDs), which typically comprise a mass, springs, and a dashpot, are one of the most traditional vibration control devices (Shi *et al.* 2018a). The primary structure is subjected to a reverse inertial force by the mass, and the vibration energy is dissipated through its dashpot. Compared to other dampers, because of the small size and minimal interference to the primary structure, TMDs are widely used in the vibration control of different structures. According to its application range, traditional TMDs can be either vertical or horizontal. Horizontal TMDs are typically used to protect tall buildings from wind loads and earthquake excitations (Nagarajaiah 2009), while vertical TMDs are typically applied in vibration control problems of footbridges and floor structures (Shi *et al.* 2018a). As the control can be divided into passive, active, semi-active and hybrid controls, TMDs can also be divided into passive, active, semi-active, and hybrid TMDs (Spencer and Nagarajaiah 2003, Wang *et al.* 2018).

As no external power source is needed, passive TMDs have a wide range of engineering applications (Wang and Lin 2015, Lu *et al.* 2017). The pendulum TMD, whose frequency is dependent on the length of the pendulum, is typically used in horizontal vibration control of tall buildings. Numerous new types of pendulum TMDs have been proposed recently, including the adaptive passive PTMD (Roffel *et al.* 2011, Wang *et al.* 2019) and mass-uncertain rolling-pendulum TMD (Emiliano and Almessandro 2009). To obtain effective control of passive TMDs, their parameters need to be well designed (Chung *et al.* 2013). However, passive TMDs are sensitive to the detuning effect and could not retune themselves, both of which would decrease their vibration control effect (Nagarajaiah and Sonmez 2007). Earthquake resistance is a critical aspect of structures; however, passive TMDs may not perform well in earthquake resistance (Sun *et al.* 2013, Domizio *et al.* 2015, Ramezani *et al.* 2017).

Semi-active TMDs can vary their parameters in real-time to improve the control effect, requiring a minimum of power to achieve this. Therefore, they are more maintainable, reliable, and stable than active TMDs (Casciati and Ubertini 2008, Sun 2018). Recently, numerous

*Corresponding author, Professor,
E-mail: yingzhou@tongji.edu.cn
[a] Ph.D. Student, E-mail: wangliangkun@tongji.edu.cn
[b] Professor, E-mail: swxtgk@tongji.edu.cn
[c] Ph.D. Student, E-mail: 2151xanxus@tongji.edu.cn

ISSN: 1738-1584 (Print), 1738-1991 (Online)

novel semi-active TMDs have been proposed (Nagarajaiah and Varadarajan 2005, Eason *et al.* 2013, Contreras *et al.* 2014, Pasala and Nagarajaiah 2014, Lin *et al.* 2015, Dinh *et al.* 2016). Varadarajan and Nagarajaiah (2004) proposed a variable stiffness TMD using empirical mode decomposition/Hilbert transform to control the wind response of a building. The Hilbert-Huang transformation (HHT) was recently developed and has numerous applications in analyzing nonlinear and nonstationary signals (Shi *et al.* 2012). Sun and Nagarajaiah (2014) presented a semi-active TMD with variable damping and stiffness to control seismic responses. Although it was a significant contribution to the semi-active and earthquake engineering fields, power analyses were not presented in this study, and only a linear structure was considered.

Eddy current damping is a type of damping resulting from the relative motion between permanent magnets and conductive plates (Lu *et al.* 2017). The Lorentz force in the conductive plate will restrict their relative motion, and the vibration energy of the damper will be dissipated by the heat of the conductive plate. Compared to a traditional TMD, the dashpot of the eddy current TMD provides eddy current damping instead of oil damping. Compared to oil damping, eddy current damping has numerous advantages, such as being suitable for assembly line production, environmentally friendly, economical, and easy adjustment of the damping ratio (Wang *et al.* 2012). Lu *et al.* (2018) proposed a shaking table test of a steel frame structure with an eddy current TMD. Shi *et al.* (2018b) proposed a vertical semi-active eddy current TMD with variable damping to control human-induced vibrations for footbridges. However, to date, there has been no research on studying a semi-active eddy current TMD for horizontal vibration control of structures.

For semi-active control, a linear system is usually used as a primary structure. However, some structures have nonlinear characteristics. Under strong earthquakes, structures will go into the nonlinear state. For most civil structures, the nonlinearity is characterized by hysteresis behaviour which can be represented by the Bouc-Wen model (Waubke and Kasess 2017, Maiti *et al.* 2018). However, there are still few researches about the passive and semi-active control of a nonlinear structure based on the Bouc-Wen model.

A novel semi-active eddy current pendulum tuned mass damper (SAEC-PTMD) with variable frequency and damping is proposed in this study. The frequency of the SAEC-PTMD is retuned through a HHT-based control algorithm by adjusting the pendulum length, and its damping is adjusted in real-time through a linear-quadratic-Gaussian (LQG)-based control algorithm. The effect of the SAEC-PTMD is verified through harmonic excitations and near-fault pulse-like earthquake excitations, for a linear and a nonlinear primary structure respectively. An optimal passive TMD is used for comparison, and its off-tune effect is considered when the structural natural frequency changed because of the cumulative damage.

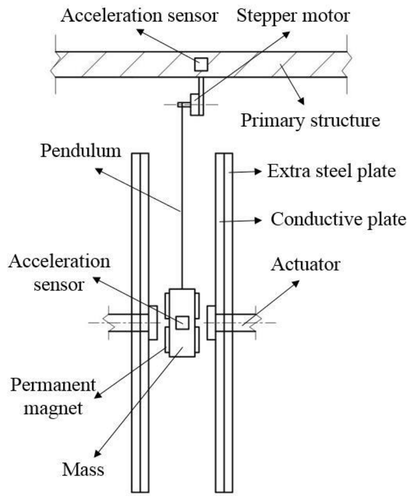

Fig. 1 SAEC-PTMD

2. Mechanical and dynamic analysis of SAEC-PTMD

2.1 Mechanical description of SAEC-PTMD

To satisfy the requirement of adjusting the pendulum and eddy current damping in real-time, a feasible schematic of an SAEC-PTMD is shown in Fig. 1.

It can be seen in Fig. 1 that many permanent magnets are located on the left and right sides of the mass, with an air gap on either side of the mass, beyond which are conductive plates and extra steel plates. The SAEC-PTMD is used to control the structural vibration in a direction perpendicular to the paper; therefore, there are separate acceleration sensors on the mass and primary structure in this direction. A computer receives signals from the two acceleration sensors and controls the stepper motor to adjust the pendulum and actuator to adjust the air gap between the conductive plate and permanent magnets; this would adjust the eddy current damping according to the HHT-based control algorithm and LQG-based control algorithm, respectively. In this manner, the SAEC-PTMD could retune itself and adjust its damping ratio in real-time.

2.2 Dynamic analysis of single-degree-of-freedom system coupled with SAEC-PTMD

The two-degree-of-freedom dynamic system comprises a single-degree-of-freedom (SDOF) primary structure and an SAEC-PTMD. This dynamic system excited by the ground motion, $\ddot{u}_g$, is shown in Fig. 2.

The motion equations of Fig. 2(a) can be written as follows

$$\begin{pmatrix} m_p & 0 \\ 0 & m_s \end{pmatrix}\begin{pmatrix} \ddot{u}_p \\ \ddot{u}_s \end{pmatrix}+\begin{pmatrix} c_p+c(t) & -c(t) \\ -c(t) & c(t) \end{pmatrix}\begin{pmatrix} \dot{u}_p \\ \dot{u}_s \end{pmatrix} + \begin{pmatrix} k_p+k(t) & -k(t) \\ -k(t) & k(t) \end{pmatrix}\begin{pmatrix} u_p \\ u_s \end{pmatrix}=\begin{pmatrix} m_p \\ m_s \end{pmatrix}\ddot{u}_g \tag{1}$$

(a) Linear primary system (b) Nonlinear primary system

Fig. 2 SDOF system coupled with SAEC-PTMD under ground motion

where m_p and m_s are the masses of the primary structure and SAEC-PTMD, respectively, c_p and $c(t)$ are the damping coefficients of the primary structure and SAEC-PTMD, respectively, k_p and $k(t)$ are the stiffness coefficients of the primary structure and SAEC-PTMD, respectively, and u_p and u_s are the absolute displacements of the primary structure and SAEC-PTMD, respectively. The overdot indicates the derivative with respect to time.

In Fig. 2(b), the Bouc-Wen hysteresis model is presented by the following equation

$$R_p = \alpha k_p u(t) + (1-\alpha) k_p z(t) \tag{2}$$

$$\dot{z}(t) = A\dot{u}(t) - \gamma|\dot{u}(t)||z(t)|^{n-1} z(t) - \theta\dot{u}(t)|z(t)|^n \tag{3}$$

where R_p is the resilience of the primary structure, α is the factor of linear resilience as a percentage of total resilience, $z(t)$ and $u(t)$ are the stress proportional displacement and relative displacement respectively. A, γ, n and θ are hysteretic parameters of the Bouc-Wen model respectively.

3. HHT-based control algorithm

3.1 Hilbert-Huang transformation

To identify the instantaneous frequency of the primary structure, HHT is used in this section.

The HHT method has numerous applications in analyzing nonlinear and nonstationary signals and can be divided into two steps: empirical mode decomposition (EMD) whereby a complicated vibration signal can be turned into a series of intrinsic mode functions (IMFs) through EMD (Shi *et al.* 2012) and performing the Hilbert transform (HT) on each IMF component (Nagarajaiah 2009). With HT, a vibration signal $Y(t)$ for a real-valued function $x(t)$ can be written as follows

$$Y(t) = x(t) + i\tilde{x}(t) = A(t)e^{-i\,\theta(t)} \tag{4}$$

$$\tilde{x}(t) = HT[\,x(t)] = \frac{1}{\pi} P \int_{-\infty}^{\infty} \frac{x(\tau)}{t-\tau} d\tau \tag{5}$$

$$A(t) = [x^2(t) + \tilde{x}^2(t)]^{\frac{1}{2}} \tag{6}$$

$$\theta(t) = arctan\left(\frac{\tilde{x}(t)}{x(t)}\right) \tag{7}$$

where i is the imaginary unit, $\tilde{x}(t)$ is the HT of $x(t)$, $A(t)$ and $\theta(t)$ are the amplitude and instantaneous phase angle of $x(t)$ respectively, and P is the Cauchy principal component.

The instantaneous frequency $f(t)$ is the time derivative of $\theta(t)$ and is shown below

$$f(t) = \frac{1}{2\pi}\frac{d\theta(t)}{\mathrm{dt}} \tag{8}$$

The vibration signal $Y(t)$ of the primary structure is obtained from the acceleration sensor on the structure, and the computer calculates the instantaneous frequency $f(t)$ of $Y(t)$.

3.2 Variable frequency control algorithm

When considering function restrictions of the components, including the primary structure, computer, and stepper motor, it is unreasonable to continuously retune the frequency of the SAEC-PTMD to the identified instantaneous frequency $f(t)$. Therefore, a frequency adjustment range (f_{min},f_{max}) should first be programmed into the computer. When $f(t)$ is greater than the preset maximum frequency, f_{max}, or smaller than the preset minimum frequency, f_{min}, the stepper motor will retune the frequency of the SAEC-PTMD $f_s(t)$ to the primary structural natural frequency f_p; otherwise, the stepper motor will retune the SAEC-PTMD to $f(t)$.

Over the full life cycle of the primary structure, it could be subjected to numerous hazards and its stiffness would decrease because of the cumulative damage. This would result in the natural frequency also decreasing. To improve the control effect of the SAEC-PTMD and consider the frequency variation in the primary structure, after a given time (for instance one month), the computer will identify the structural natural frequency from the acceleration signal of the primary structure under ambient excitation. The f_p will be then updated to the new frequency. If the new identified natural frequency of the primary structure is greater than f_{max} or smaller than f_{min}, f_p will be updated to f_{max} or f_{min}.

The relationship between the length of the pendulum, $L(t)$, and the frequency of the SAEC-PTMD, $f_s(t)$, can be written as follows

$$L(t) = \frac{g}{4\pi^2 f_s(t)^2} \tag{9}$$

From Eq. (9), the SAEC-PTMD can easily be retuned by controlling the stepper motor to adjust the pendulum length in real-time.

4. LQG-based control algorithm

In Fig. 1, a computer receives signals from two acceleration sensors and controls the actuator to adjust the air gap between the conductive plate and permanent magnets, which is the semi-active eddy current damping, according to LQG-based control algorithm. Therefore, in this section, the relationship between effective damping coefficients and the air gap will first be fitted with a polynomial function. The LQG-based control algorithm will then be introduced.

4.1 Eddy current damping

Eddy current damping is typically created by the relative motion between magnets and conductive plates. If the direction of movement of the conductive plates is perpendicular to the direction of the magnetic induction intensity, $\boldsymbol{B_x}$, the Lorentz force $\boldsymbol{F_x}$ can be written as follows

$$\boldsymbol{F_x} = \int_V J \times \boldsymbol{B_x} dV = \int_V \sigma(V \times \boldsymbol{B_x}) \times \boldsymbol{B_x} dV = -\sigma\delta S {\boldsymbol{B_x}}^2 \boldsymbol{v} \tag{10}$$

where J represents the electric current density, V is the relative velocity of the magnet to the conductive plate, σ is the conductive coefficient of the conductive plate, δ is the thickness of the conductive plate, S can be simplified as the area of the magnet projected onto the conductor plate, and $\boldsymbol{v}$ is the relative velocity between the magnets and conductive plates. A linear damping coefficient, c_x, in this direction can then be written as

$$c_x = \sigma\delta S {B_x}^2 \tag{11}$$

where B_x is the magnetic induction intensity that is dependent on the adsorption positions of the magnets, material and thickness of the conductive plates, thickness of the extra steel plates, and air gap between the magnets and conductive plates, and, therefore, B_x is difficult to determine. Consequently, the finite element (FE) model is built in Opera3D (Oxford, UK), an FE analysis software for electromagnetic fields. In the following case study, a 300 kg SDOF primary structure will be simulated and the TMD

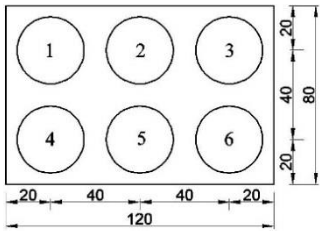

Fig. 3 Adsorption position of permanent magnets (mm)

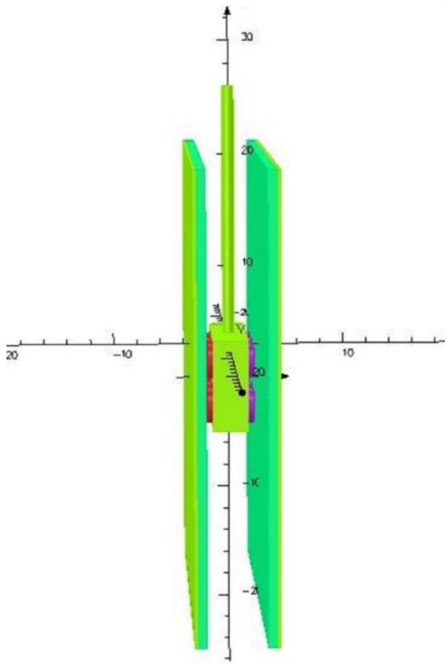

Fig. 4 FE model of SAEC-PTMD

mass ratio will be set to approximately 1%. Therefore, the mass of the SAEC-PTMD is approximately 3 kg, and it is 120-mm long, 30-mm wide, and 80-mm high.

Permanent magnets comprise N35 (NdFeB) material, with diameter of 30 mm and height of 5 mm. The conductive plates are copper, 400-mm long, and 400-mm wide. Considering the size compatibility of the magnets and mass, there are six circular permanent magnets on either side of the mass, and their adsorption arrangement is shown in Fig. 3. Different adsorption positions would lead to different magnetic induction intensities, with one of the options presented in (Shi *et al.* 2018b). The FE model of the SAEC-PTMD in Opera 3D is shown in Fig. 4.

The method to choose the combination of the thickness of copper plates and extra steel plates is the same as (Shi *et al.* 2018b). As a result, the chosen thickness of copper plates is 8 mm, and extra plates is 2 mm. When the mass is given a 30-mm/s horizontal velocity, v, the distribution of eddy current in the copper plate is shown in Fig. 5.

Shi *et al.* (2018b) proposed the distribution of eddy current in the copper plate of a vertical eddy current TMD, with two large eddy currents in the upper and lower areas of the copper plate; in Fig. 5, there are two large eddy currents on the left- and right-hand sides of the copper plate. This is caused by the difference in the relative motion direction.

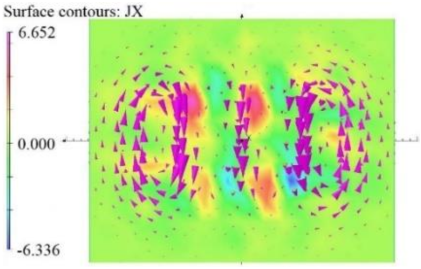

Fig. 5 Distribution cloud picture of electric current density (A/cm^2)

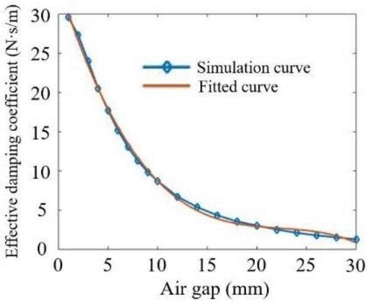

Fig. 6 Effective damping coefficient as function of air gap and fitting curve

A detailed discussion of the loss of eddy current damping can be found elsewhere.

4.2 Discussion on the effect of air gap

The damping of the SAEC-PTMD is adjusted in real-time by adjusting the air gap between the conductive plate and permanent magnets. Therefore, the relationship between effective damping coefficients and the air gap is discussed in this section. Air gaps from 1 mm are used, and the mass is given a 30-mm/s horizontal velocity. The resulting effective damping coefficients are presented in Table 1.

The relationship between the effective damping coefficient of SAEC-PTMD, $c_s(x)$, and the air gap, x, is fitted through a polynomial function

$$c_s(x) = -2.627 \times 10^{-3}x^3 + 0.176x^2 - 4.022x + 33.950 \tag{12}$$

The effective damping coefficient as a function of the air gap and the fitting curve are shown in Fig. 6, where it can be seen that the two curves are in good agreement. With this fitting function, the damping ratio of the SAEC-PTMD can be easily adjusted by adjusting the air gap in real-time.

4.3 Variable damping control algorithm

For actual civil engineering applications, the acceleration sensor is one of the most economical and practical sensors, and the displacement and velocity feedback can be integrated from the acceleration signal. The LQG control algorithm has a wide application in active control of civil structures. One of the advantages of LQG control is that it only needs acceleration signals and, consequently, the control devices can be simplified. The external force is assumed to be a zero-mean white noise process with Gaussian distribution and constant covariance. The Kalman filter is used as an observer to estimate full states of the dynamic system.

As discussed above, a computer receives the two acceleration sensor signals and controls the actuator in real-time that can adjust the air gap between the copper plates and the permanent magnets by attracting and repulsing the copper plates. The semi-active variable damping control algorithm is the LQG-based control algorithm.

The active control force, $u(t)$, is obtained through minimizing the following quadratic expression of the cost function (Shi *et al.* 2018b)

$$J_c = \lim_{T\to\infty} \frac{1}{T}\int_0^T [U^T(t)QU(t) + u^T(t)Ru(t)]dt \tag{13}$$

where J_c is the cost function, $\boldsymbol{U(t)}$ is the state vector of the dynamic system, $\boldsymbol{Q}$ is a positive semi-definite weighting matrix, $\boldsymbol{R}$ is a positive weighting matrix, and T is the total calculation time. After the trial, it is chosen that $\boldsymbol{Q} = 10^5[I]$ and $\boldsymbol{R} = (\frac{1}{100})[I]$, where I is an identity

Table 1 Effective damping coefficient as function of air gap

Case	Air gap/mm	Effective damping coefficient c_e/(N·s/m)	Case	Air gap/mm	Effective damping coefficient c_e/(N·s/m)
1	1	29.603	11	12	6.730
2	2	27.298	12	14	5.377
3	3	23.981	13	16	4.352
4	4	20.541	14	18	3.570
5	5	17.728	15	20	3.032
6	6	15.186	16	22	2.532
7	7	13.058	17	24	2.126
8	8	11.287	18	26	1.787
9	9	9.866	19	28	1.528
10	10	8.706	20	30	1.298

matrix.

As for the SAEC-PTMD, $u(t)$ is provided by the semi-active eddy current damping, $c(t)$, which can be written as

$$c(t) = u(t)/\dot{u}_s \tag{14}$$

where $\dot{u}_s$ is the velocity of the SAEC-PTMD.

Considering that the required control force calculated from the LQG algorithm could exceed the damping adjustment range that the SAEC-PTMD can accommodate, the following boundary is set

$$c(t) = \begin{cases} c_{max} & c_{max} \leq c(t) \\ c(t) & c_{max} > c(t) > c_{min} \\ c_{min} & c_{min} \geq c(t) \end{cases} \tag{15}$$

where c_{max} is the maximum of the variable damping coefficient, and c_{min} is the minimum of the variable damping coefficient. In the following case study, c_{max} is set as 29.6 N·s/m according to Table 1, and c_{min} is set as 0.

It has been verified that no extra stiffness will be induced from eddy current damper at any working frequency of TMD (Wang *et al.* 2012), and it is said in (Lu *et al.* 2018) that the eddy current TMD is primarily used for adjusting the damping properties of the auxiliary mass; however, it is not providing stiffness tuning. Therefore, in the following, the electromagnetic field's further nonlinear contribution to the stiffness of the pendulum is ignored. Besides, the dynamics of the stepper motor and the actuator for the conductive plate are ignored in the numerical simulation, and the time-delay effect is ignored either.

5. Case study: Linear structure

In this section, a linear primary structure, as proposed in Fig. 2(a), coupled with different TMDs will be considered. In the following simulations, the sample frequency is set to be 1000 Hz, and the retuning frequency of SAEC-PTMD is 50 Hz. The pendulum is tuned to the average frequency of each cycle.

A 300 kg SDOF primary structure, with a 1.0 Hz natural frequency and 2.0% damping ratio coupled with an SAEC-PTMD, will be simulated under harmonic excitations, white noise excitation, and earthquake excitations. The pendulum adjustment range of the SAEC-PTMD is set as (15.94 cm, 35.94 cm), implying that the frequency adjustment range of SAEC-PTMD is 0.84–1.26 Hz. An optimal passive TMD is used for comparison and for the previous two types of excitation. The PTMD is optimized as follows (Den Hartog 1985)

$$f_{opt} = \frac{1}{1+\mu} \tag{16}$$

$$\zeta_{opt} = \sqrt{\frac{3\mu}{8(1+\mu)}} \tag{17}$$

As for earthquake excitations, the PTMD is optimized as follows (Sun and Nagarajaiah 2014)

$$f_{opt2} = \frac{1}{1+\mu_p}\left(1 - \zeta_p\sqrt{\frac{\mu}{1+\mu}}\right) \tag{18}$$

$$\zeta_{\mathrm{opt2}} = \frac{\zeta_p}{1+\mu} + \sqrt{\frac{\mu}{1+\mu}} \tag{19}$$

In Eqs. (16)-(19), the TMD mass ratio, μ, is set as 1%. Therefore, according to Eqs. (16) and (17), for harmonic excitations and white noise excitation, the TMD optimal frequency ratio and damping ratio are 0.99% and 6.09%, respectively. According to Eqs. (18) and (19), for earthquake excitations, the TMD optimal frequency ratio and damping ratio are 0.99% and 11.93%, respectively. In order to consider the cumulative damage of primary structures and the detuning effect of the PTMD, the natural frequency of the primary structure is set as 0.90 Hz.

Under white noise excitation, the 40-s-long acceleration signal of the primary structure coupled with an SAEC-PTMD is analyzed through fast-Fourier transform (FFT). For actual applications, other means of frequency identification could have higher precision. The identified structural natural frequencies of the 1.0 Hz and 0.9 Hz structures are 0.99 Hz and 0.89 Hz, respectively. Because they are in the frequency adjustment range, the f_p in section 3 will be updated accordingly.

Table 2 Performance assessment for harmonic excitation simulations

Simulation conditions		No TMD	PTMD	SAEC-PTMD	Reduction (%)	
					No TMD	PTMD
Maximum acceleration (m/s^2)	1.0 Hz harmonic excitation for 1.00 Hz structure	24.84	8.32	4.72	81.00	43.27
	0.9 Hz harmonic excitation for 0.9 Hz structure	24.74	13.43	5.23	78.86	61.06
Maximum displacement (cm)	1.0 Hz harmonic excitation for 1.0 Hz structure	62.84	20.98	11.90	81.06	43.28
	0.9 Hz harmonic excitation for 0.90 Hz structure	77.27	41.92	16.42	78.75	60.83
Maximum acceleration dynamic amplification factor	1.0 Hz structure	25.00	9.96	4.40	82.40	55.82
	0.9 Hz structure	25.00	17.67	4.79	80.84	72.89
Maximum displacement dynamic amplification factor	1.0 Hz structure	25.00	9.71	4.62	81.52	52.42
	0.9 Hz structure	25.00	18.49	5.00	80.00	72.96

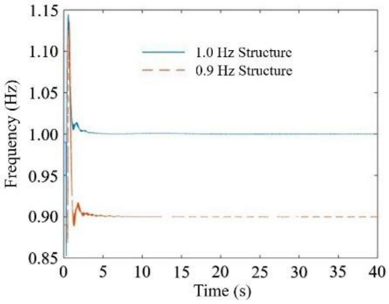

(a) Instantaneous frequency

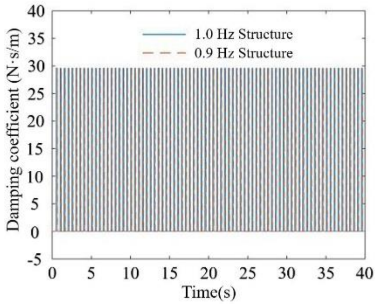

(b) Semi-active eddy current damping

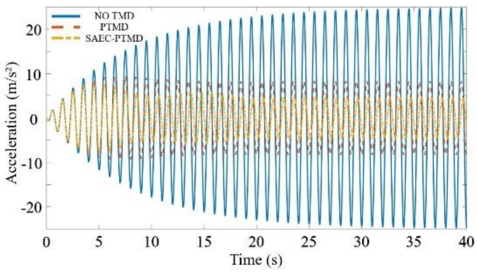

(c) Acceleration of 1.0 Hz structure under 1.0 Hz harmonic excitation

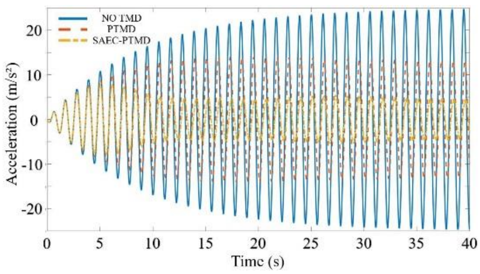

(d) Acceleration of 0.9 Hz structure under 0.9 Hz harmonic excitation

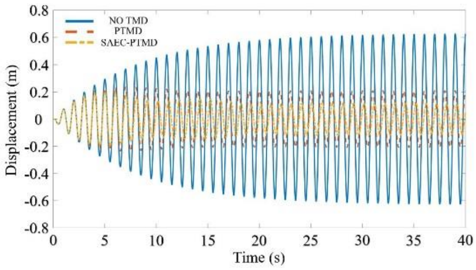

(e) Displacement of 1.0 Hz structure under 1.0 Hz harmonic excitation

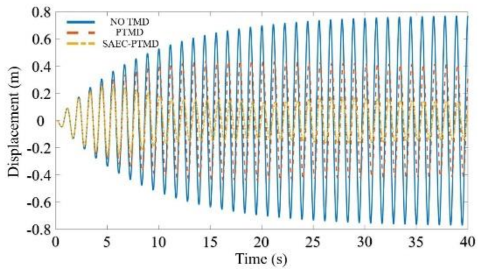

(f) Displacement of 0.9 Hz structure under 0.9 Hz harmonic excitation

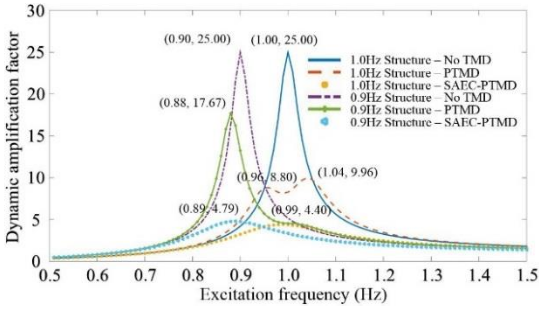

(g) Acceleration dynamic amplification factor under different-frequency harmonic excitations

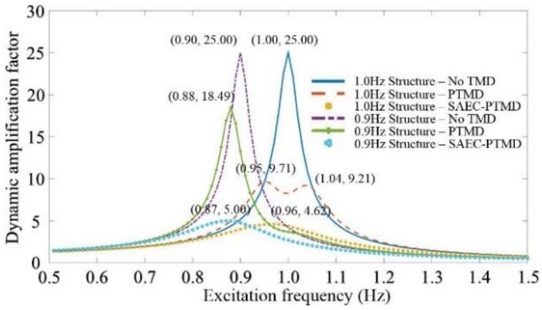

(h) Displacement dynamic amplification factor under different-frequency harmonic excitations

Fig. 7 Comparisons of harmonic excitation condition

5.1 Harmonic excitation comparison simulation

The 1.0 Hz primary structure with no TMD, coupled with a PTMD/SAEC-PTMD is excited by a 1.0 Hz harmonic excitation, and the 0.9 Hz primary structure with no TMD, coupled with a PTMD/SAEC-PTMD, is excited by a 0.9 Hz harmonic excitation. The results are shown in Fig. 7 and Table 2. The maximum harmonic excitations are set as 1.0 m/s^2.

As can be seen from Fig. 7(a), after the first three seconds, the primary structure enters a steady vibration state, and the instantaneous frequency of the primary structure is steady at 1.0 Hz/0.9 Hz. It can be seen from Fig. 7(b) that the damping coefficient of SAEC-PTMD varies in the adjustment range (0, 29.6 N·s/m). From Figs. 7(c)-(f) and Table 2, it can be concluded that the SAEC-PTMD performs significantly better than the no TMD and PTMD cases, and, when the PTMD is mistuned, the SAEC-PTMD could retune itself to restore the vibration control effect. It can be seen in Figs 7(g) and (h) that in several ranges that deviate from the resonance range, the dynamic amplification factors of PTMD are marginally greater than the no TMD case, both for the 1.0 Hz and 0.9 Hz structures. However, the SAEC-PTMD never has a negative effect.

5.2 Earthquake excitation comparison simulation

Four near-fault pulse-like earthquakes with different site-characteristic periods are chosen to examine the effectiveness of the SAEC-PTMD against PTMD. The data of the four selected earthquake excitations are presented in Table 3. The maximum values of the four earthquake excitations are set as 10.0 m/s^2.

The 1.0 Hz/0.9 Hz primary structures with no TMD, coupled with a PTMD/SAEC-PTMD, are excited by four earthquake excitations, and the results are presented in Fig. 8 and Table 4. The structural acceleration and displacement response spectra under the four earthquake excitations are shown in Fig. 9.

From Figs. 8 and 9, and Table 4, it can be concluded that for different earthquake excitations, the tendencies are different, but in general, the SAEC-PTMD performs better than PTMD, and the RMS reductions are greater than the maximum. The SAEC-PTMD could attenuate acceleration and displacement spectra over a wide range of periods compared to the no TMD and PTMD cases under all four earthquake excitations.

To further study the performance of the SAEC-PTMD under earthquake excitations, structural responses under the Northridge earthquake excitation will be analyzed as an

Table 3 The information of selected near-fault earthquake excitations

No.	T_p (s)	Earthquake location	Year	Station name	Magnitude	Mechanism	R_{jb} (km)	R_{rup} (km)
1	0.588	Northridge	1994	Pacoima Dam	6.69	Reverse	4.92	7.01
2	1.092	Kobe, Japan	1995	KJMA	6.90	Strike slip	0.94	0.96
3	1.568	Loma Prieta	1989	Los Gatos-Lexington Dam	6.93	Reverse oblique	3.22	5.02
4	2.570	Chi-Chi, Taiwan	1999	CHY006	7.62	Reverse oblique	9.76	9.76

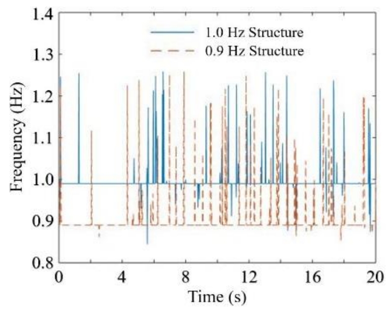

(a) Instantaneous frequency

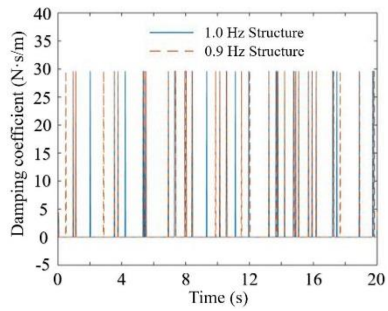

(b) Semi-active eddy current damping

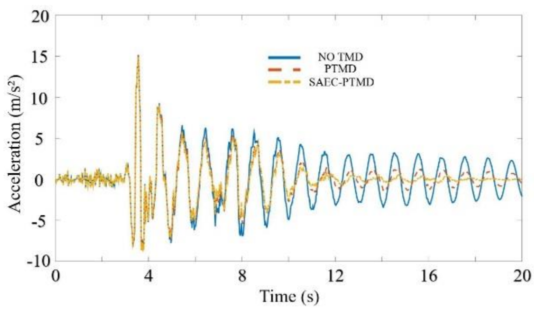

(c) Acceleration of 1.0 Hz structure

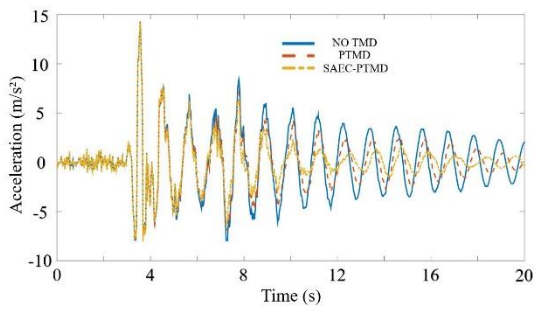

(d) Acceleration of 0.9 Hz structure

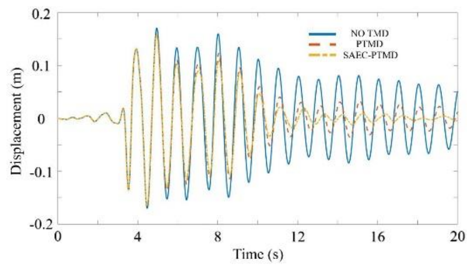

(e) Displacement of 1.0 Hz structure

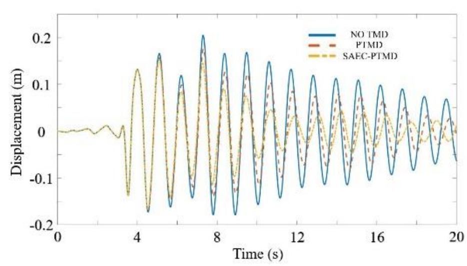

(f) Displacement of 0.9 Hz structure

Fig. 8 The comparisons of Northridge earthquake excitation condition

Table 4 Performance assessment for earthquake excitation simulations

Northridge		Acceleration (m/s^2)				Displacement (cm)			
		Maximum		RMS		Maximum		RMS	
		1.0 Hz structure	0.9 Hz structure	1.0 Hz structure	0.9 Hz structure	1.0 Hz structure	0.9 Hz structure	1.0 Hz structure	0.9 Hz structure
No TMD		15.16	14.29	3.17	3.18	17.07	20.50	7.07	8.59
PTMD		15.15	14.29	2.56	2.63	16.54	17.58	5.25	6.71
SAEC-PTMD		14.91	14.13	2.42	2.26	16.48	16.70	4.83	5.20
Reduction (%)	No TMD	1.65	1.12	23.66	28.93	3.46	18.54	31.68	39.46
	PTMD	1.58	1.12	5.47	14.07	0.36	5.01	8.00	22.50
Kobe, Japan		Acceleration (m/s^2)				Displacement (cm)			
		Maximum		RMS		Maximum		RMS	
		1.0 Hz structure	0.9 Hz structure	1.0 Hz structure	0.9 Hz structure	1.0 Hz structure	0.9 Hz structure	1.0 Hz structure	0.9 Hz structure
No TMD		24.82	19.50	5.03	2.68	52.45	49.94	12.18	6.95
PTMD		24.28	19.25	3.67	2.50	51.22	48.38	8.48	6.47
SAEC-PTMD		23.82	17.78	3.45	2.44	50.85	45.81	8.12	6.31
Reduction (%)	No TMD	4.03	8.82	31.41	8.96	3.05	8.27	33.33	9.21
	PTMD	1.89	7.64	5.99	2.40	0.72	5.31	4.25	2.47
Loma Prieta		Acceleration (m/s^2)				Displacement (cm)			
		Maximum		RMS		Maximum		RMS	
		1.0 Hz structure	0.9 Hz structure	1.0 Hz structure	0.9 Hz structure	1.0 Hz structure	0.9 Hz structure	1.0 Hz structure	0.9 Hz structure
No TMD		38.01	35.70	6.33	6.42	92.87	99.20	15.95	19.63
PTMD		33.40	32.82	4.68	5.04	82.73	91.79	11.82	15.58
SAEC-PTMD		30.70	32.12	4.40	4.23	79.82	88.70	11.34	12.78
Reduction (%)	No TMD	19.23	10.03	30.49	34.11	14.05	10.58	28.90	34.90
	PTMD	8.08	2.13	5.98	16.07	3.52	3.37	4.06	17.97
Chi-Chi, Taiwan		Acceleration (m/s^2)				Displacement (cm)			
		Maximum		RMS		Maximum		RMS	
		1.0 Hz structure	0.9 Hz structure	1.0 Hz structure	0.9 Hz structure	1.0 Hz structure	0.9 Hz structure	1.0 Hz structure	0.9 Hz structure
No TMD		31.52	30.86	5.64	5.89	79.36	81.11	14.19	18.21
PTMD		28.42	27.92	4.17	4.82	72.25	71.92	10.62	15.19
SAEC-PTMD		25.97	26.84	3.95	3.87	66.46	70.97	9.99	11.70
Reduction (%)	No TMD	17.61	13.03	29.96	34.30	16.26	12.50	29.60	35.75
	PTMD	8.62	3.87	5.28	19.71	8.01	1.32	5.93	22.98

example below, from the perspective of energy dissipation. The comparisons of the hysteresis loops of PTMD and SAEC-PTMD in the 1.0 Hz/0.9 Hz structures under the Northridge earthquake excitation are shown in Fig. 10.

It can be seen in Fig. 10 that the hysteresis loops of the SAEC-PTMD are greater than for the PTMD, and for the 0.9 Hz structure, the hysteresis loops of SAEC-PTMD are significantly greater, implying that the SAEC-PTMD has a better energy dissipation capacity than the PTMD. The spikes in the hysteresis loops of the SAEC-PTMD are caused by rapid changes in the frequency and damping coefficients. The comparisons of the input energy and dissipated energy under the Northridge earthquake excitation are presented in Table 5.

In Table 5, E_I is the input energy of the earthquake, and E_S is the energy dissipated by the PTMD/SAEC-PTMD. As can be seen from Table 5, the input energy of the primary structure with an SAEC-PTMD is the smallest for both the 1.0 Hz and 0.9 Hz structures; however, the energy dissipated by the SAEC-PTMD is greater than that of the PTMD for both the 1.0 Hz and 0.9 Hz structures, which further illustrates the better control effect and energy dissipation capacity of the SAEC-PTMD.

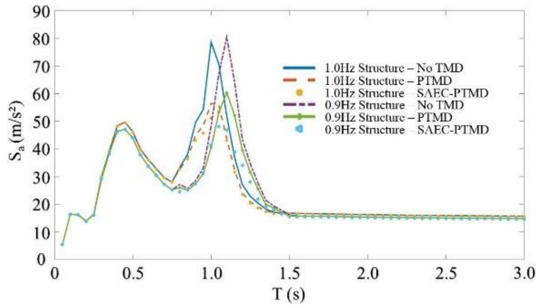

(a) Structural acceleration response spectra under Northrid geearthquake

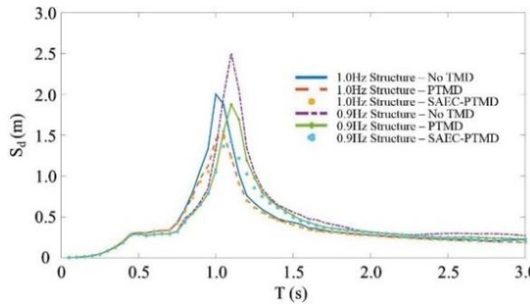

(b) Structural displacement response spectra under Northridge earthquake

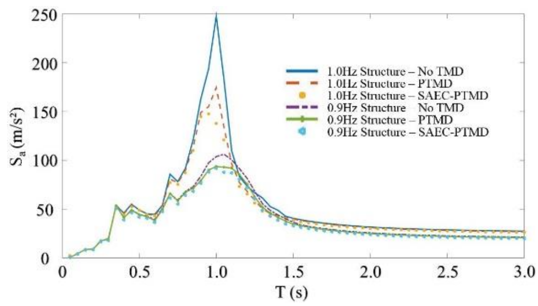

(c) Structural acceleration response spectra under Kobe earthquake

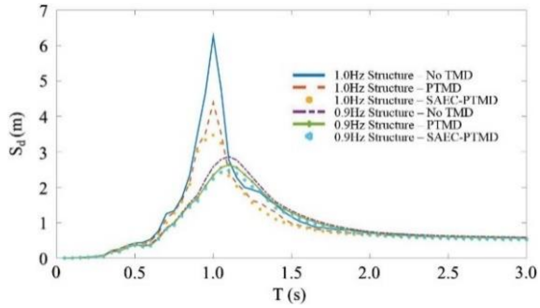

(d) Structural displacement response spectra under Kobe earthquake

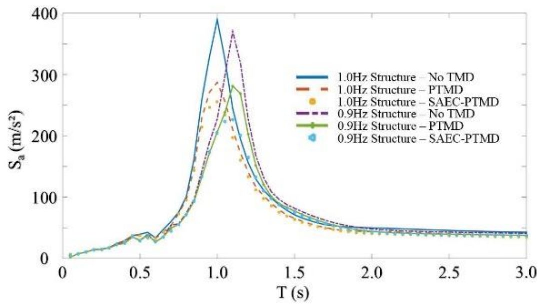

(e) Structural acceleration response spectra under Loma Prieta earthquake

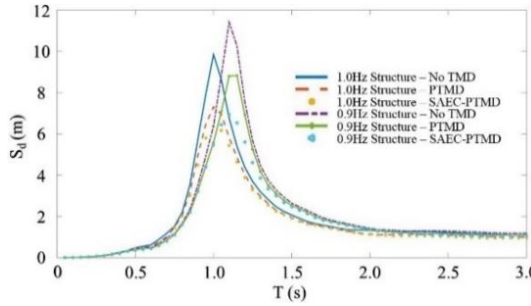

(f) Structural displacement response spectra under Loma Prieta earthquake

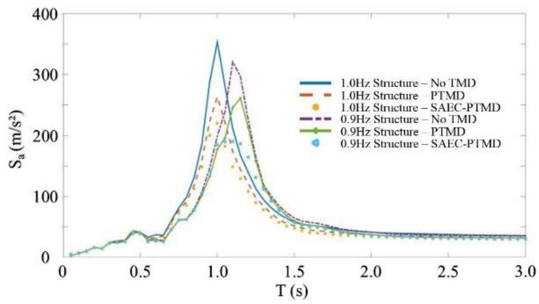

(g) Structural acceleration response spectra under Chi-Chi earthquake

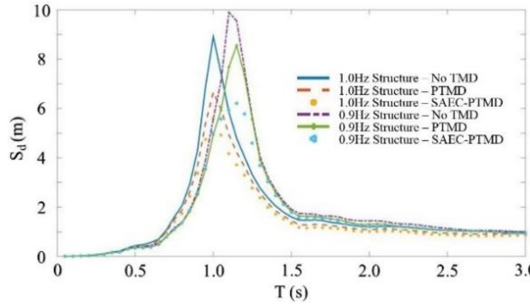

(h) Structural displacement response spectra under Chi-Chi earthquake

Fig. 9 Structural acceleration and displacement response spectra under four selected earthquakes

6. Case study: Nonlinear structure

As for the nonlinear primary structure, without loss of generality, in Eqs. (2) and (3), parameters α, A, γ, n and θ are set to be 0.4, 0.5, 0.5, 3 and 1 respectively. Other parameters of the primary structure and TMDs are all the same as section 5. It should be noticed that in the following, in order to be consistent with section 5, “1.0 Hz structure” means that the frequency calculated from nonlinear primary structural linear stiffness coefficient and mass is 1.0 Hz, and the same as “0.9 Hz structure”

6.1 Harmonic excitation comparison simulation

The dynamic responses of a nonlinear structure are not only related to the frequency of external excitation, but also

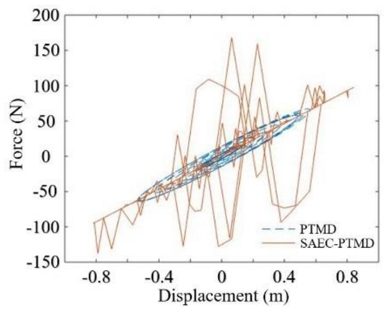

(a) Force/displacement relationship of 1.0 Hz structure

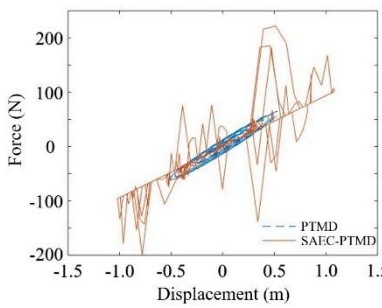

(b) Force/displacement relationship of 0.9 Hz structure

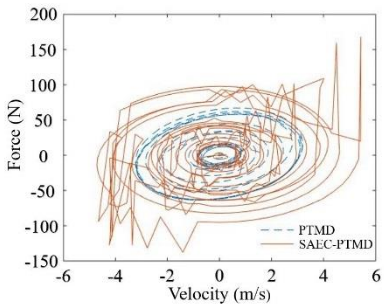

(c) Force/velocity relationship of 1.0 Hz structure

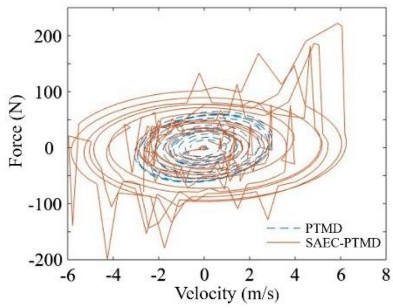

(d) Force/velocity relationship of 0.9 Hz structure

Fig. 10 Comparisons of TMD hysteresis loops under Northridge ground motion

Table 5 Performance assessment for dissipation of earthquake energy

Northridge	1.0 Hz structure			0.9 Hz structure		
	No TMD	PTMD	SAEC-PTMD	No TMD	PTMD	SAEC-PTMD
E_I (J)	1770.45	1563.89	1501.86	1753.91	1599.18	1474.04
E_S (J)		151.88	187.28		155.97	187.16
E_S/E_I (%)		9.71	12.47		9.75	12.70

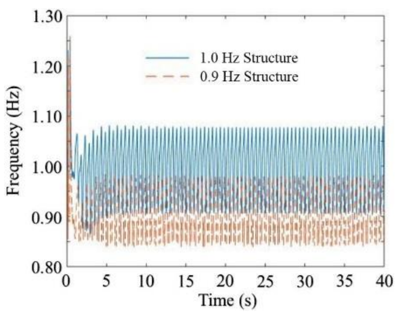

(a) Instantaneous frequency

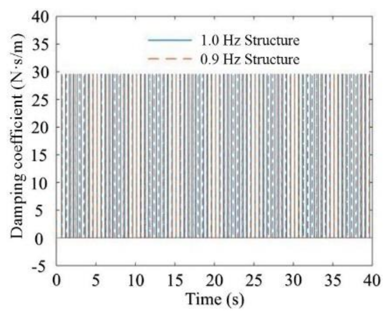

(b) Semi-active eddy current damping

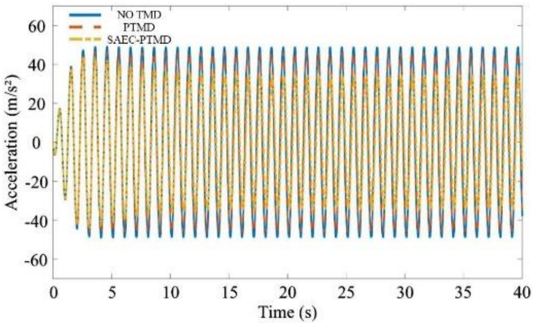

(c) Acceleration of 1.0 Hz structure under 1.0 Hz harmonic excitation

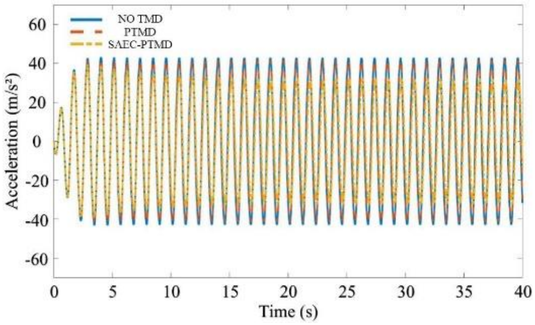

(d) Acceleration of 0.9 Hz structure under 0.9 Hz harmonic excitation

Fig. 11 Comparisons of harmonic excitation condition of the nonlinear structure

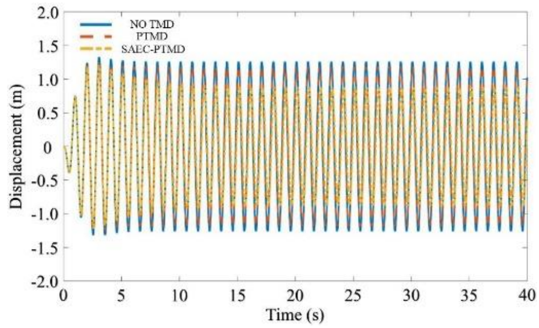

(e) Displacement of 1.0 Hz structure under 1.0 Hz harmonic excitation

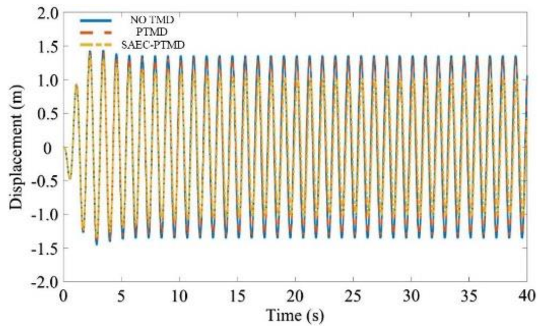

(f) Displacement of 0.9 Hz structure under 0.9 Hz harmonic excitation

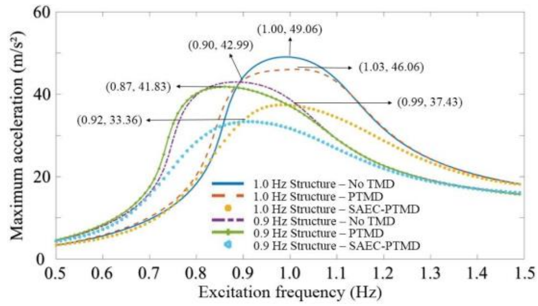

(g) Structural acceleration response spectra under Chi-Chi earthquake

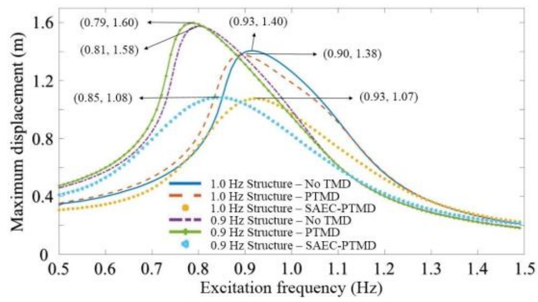

(h) Structural displacement response spectra under Chi-Chi earthquake

Fig. 11 Continued

Table 6 Performance assessment for harmonic excitation simulations of the nonlinear structure

Simulation conditions		No TMD	PTMD	SAEC-PTMD	Reduction (%)	
					No TMD	PTMD
Maximum acceleration (m/s^2)	1.0 Hz harmonic excitation for 1.0 Hz structure	49.06	46.02	34.66	29.35	24.68
	0.9 Hz harmonic excitation for 0.9 Hz structure	42.92	41.37	32.41	24.49	21.66
Maximum displacement (m)	1.0 Hz harmonic excitation for 1.0 Hz structure	1.26	1.18	0.88	30.16	25.42
	0.9 Hz harmonic excitation for 0.9 Hz structure	1.36	1.31	1.02	25.00	22.14
Maximum acceleration response (m/s^2)	1.0 Hz structure	49.06	46.06	37.43	23.71	18.74
	0.9 Hz structure	42.99	41.83	33.36	22.40	20.25
Maximum displacement response (m)	1.0 Hz structure	1.40	1.38	1.07	23.57	22.46
	0.9 Hz structure	1.58	1.60	1.08	31.65	32.50

the amplitude. Firstly, the maximum harmonic excitations are set as 10.0 m/s^2. The 1.0 Hz primary structure with no TMD, coupled with a PTMD/SAEC-PTMD is excited by a 1.0 Hz harmonic excitation, and the 0.9 Hz primary structure with no TMD, coupled with a PTMD/SAEC-PTMD, is excited by a 0.9 Hz harmonic excitation. The results are shown in Fig. 11 and Table 6.

Comparing of Figs. 7(a) and 11(a), it can be seen that for the linear primary structure, when it is excited by a harmonic excitation, the instantaneous frequency is nearly steady at a constant value. However, for the nonlinear primary structure, the instantaneous frequency is varied like a harmonic wave. Comparing of Figs. 7(g)-(h) and Figs. 11(g)-(h), it is shown that dynamic response spectra of the nonlinear primary structure is smoother than the linear one. All in all, the SAEC-PTMD has the best vibration control effect and never performs a negative effect.

To consider the influence comes from the harmonic excitation amplitude, excitation amplitude-excitation frequency-response amplitude spectrogram and the response amplitude as a function of excitation amplitude are shown in Fig. 12.

As presented in Fig. 12, the dynamic responses increment of the primary structure is nonlinear. With the increment of the excitation amplitude, the dynamic response firstly grows rapidly, and after a smooth inflection, it grows slower. No matter under which amplitude of harmonic excitation, SAEC-PTMD always has the best response control effect.

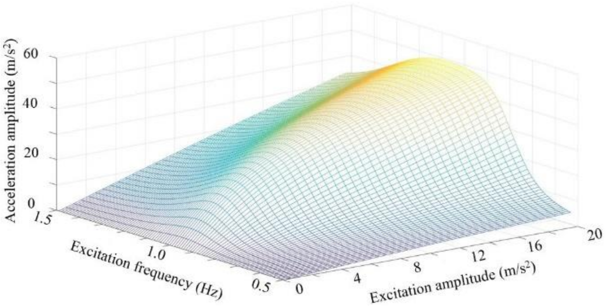

(a) Acceleration spectrogram of the 1.0 Hz structure coupled with an SAEC-PTMD

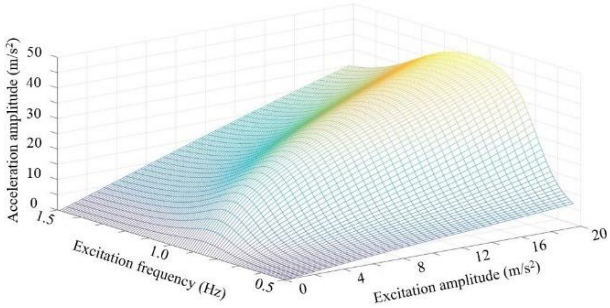

(b) Acceleration spectrogram of the 0.9 Hz structure coupled with an SAEC-PTMD

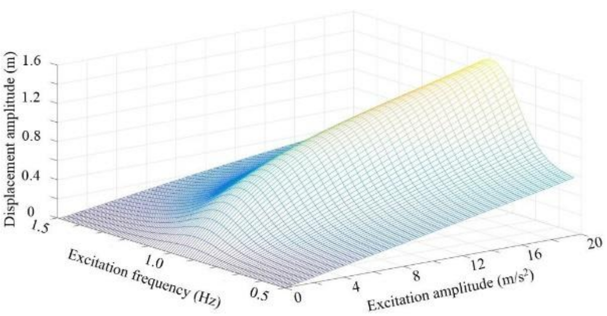

(c) Displacement spectrogram of the 1.0 Hz structure coupled with an SAEC-PTMD

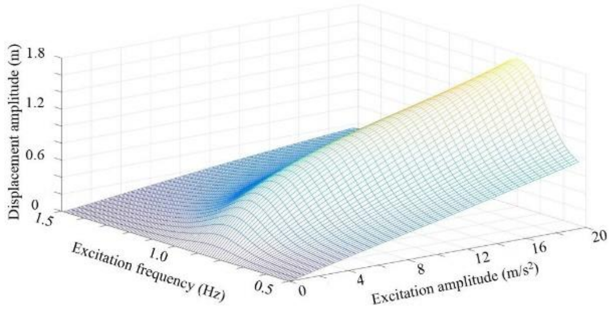

(d) Displacement spectrogram of the 0.9 Hz structure coupled with an SAEC-PTMD

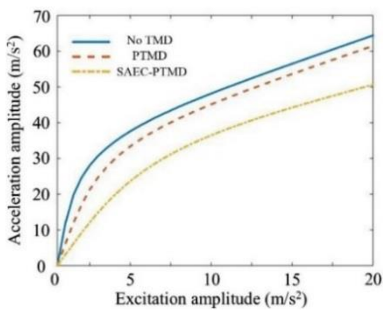

(e) Acceleration amplitude of 1.0 Hz structure under 1.0 Hz harmonic

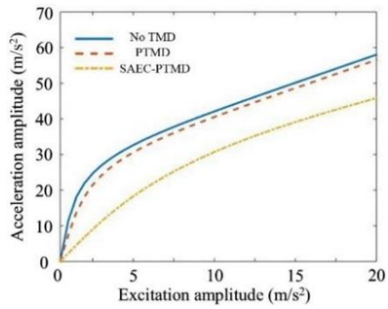

(f) Acceleration amplitude of 0.9 Hz structure under 0.9 Hz harmonic

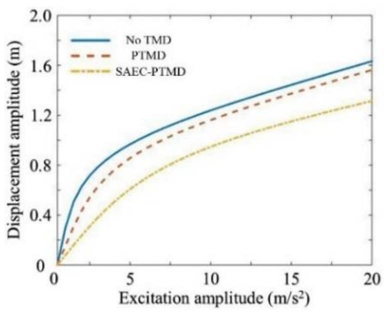

(g) Displacement amplitude of 1.0 Hz structure under 1.0 Hz harmonic

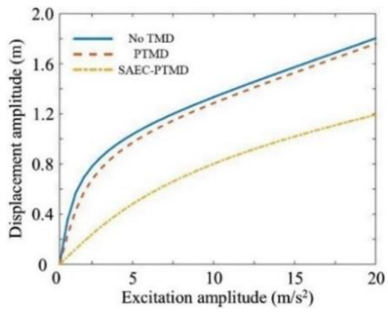

(h) Displacement amplitude of 0.9 Hz structure under 0.9 Hz harmonic

Fig. 12 Comparisons of nonlinear dynamic responses increment of the nonlinear structure

6.2 Earthquake excitation comparison simulation

To further study the performance of the SAEC-PTMD under earthquake excitations, the same as section 5, structural responses under the Northridge earthquake excitation will be analyzed as an example from the perspective of energy dissipation. The same earthquake excitations are chosen to examine the effectiveness of the SAEC-PTMD against PTMD, and the maximum values of the four earthquake excitations are also set as 10.0 m/s^2. The time history comparison results are presented in Table 7.

Comparing of Tables 7 and 4, though the earthquake excitations are totally the same, because of the different

Table 7 Performance assessment for earthquake excitation simulations of the nonlinear structure

Northridge		Acceleration (m/s^2)				Displacement (cm)			
		Maximum		RMS		Maximum		RMS	
		1.0 Hz structure	0.9 Hz structure	1.0 Hz structure	0.9 Hz structure	1.0 Hz structure	0.9 Hz structure	1.0 Hz structure	0.9 Hz structure
No TMD		14.97	14.15	3.15	3.16	17.12	20.49	7.09	8.58
PTMD		14.93	14.14	2.56	2.66	16.71	18.01	5.35	6.89
SAEC-PTMD		14.92	14.13	2.37	2.23	16.60	16.77	4.69	5.10
Reduction (%)	No TMD	0.33	0.14	24.76	29.43	3.04	18.16	33.85	40.56
	PTMD	0.07	0.07	7.42	16.17	0.66	6.89	12.34	25.98
Kobe, Japan		Acceleration (m/s^2)				Displacement (cm)			
		Maximum		RMS		Maximum		RMS	
		1.0 Hz structure	0.9 Hz structure	1.0 Hz structure	0.9 Hz structure	1.0 Hz structure	0.9 Hz structure	1.0 Hz structure	0.9 Hz structure
No TMD		24.40	18.90	4.79	2.62	52.38	49.56	11.63	6.81
PTMD		23.82	18.82	3.58	2.48	51.27	48.32	8.38	6.55
SAEC-PTMD		23.60	18.61	3.43	2.40	50.74	47.30	7.98	6.37
Reduction (%)	No TMD	3.28	1.53	28.39	8.40	3.13	4.56	31.38	6.46
	PTMD	0.92	1.12	4.19	3.33	1.05	2.11	4.77	2.75
Loma Prieta		Acceleration (m/s^2)				Displacement (cm)			
		Maximum		RMS		Maximum		RMS	
		1.0 Hz structure	0.9 Hz structure	1.0 Hz structure	0.9 Hz structure	1.0 Hz structure	0.9 Hz structure	1.0 Hz structure	0.9 Hz structure
No TMD		31.67	30.20	7.19	7.14	82.11	86.60	18.42	21.89
PTMD		29.05	28.56	5.91	6.20	77.61	82.27	15.32	19.23
SAEC-PTMD		28.43	27.63	5.68	5.47	74.05	78.24	15.00	16.91
Reduction (%)	No TMD	10.23	8.51	21.00	23.39	9.82	9.65	18.57	22.75
	PTMD	2.13	3.26	3.89	11.77	4.59	4.90	2.09	12.06
Chi-Chi, Taiwan		Acceleration (m/s^2)				Displacement (cm)			
		Maximum		RMS		Maximum		RMS	
		1.0 Hz structure	0.9 Hz structure	1.0 Hz structure	0.9 Hz structure	1.0 Hz structure	0.9 Hz structure	1.0 Hz structure	0.9 Hz structure
No TMD		29.22	27.20	4.77	4.96	75.97	70.12	12.17	15.40
PTMD		26.92	25.26	3.89	4.39	70.37	69.62	10.06	13.91
SAEC-PTMD		24.97	23.95	3.64	3.67	65.47	68.71	9.52	11.54
Reduction (%)	No TMD	14.54	11.95	23.69	26.01	13.82	2.01	21.77	25.06
	PTMD	7.24	5.19	6.43	16.40	6.96	1.31	5.37	17.04

characteristic of the primary structure, dynamic responses are different. Similar conclusions can be obtained that for different earthquake excitations, the SAEC-PTMD performs better than PTMD, and the RMS reductions are greater than the maximum. The comparisons of the resilience loops of the 1.0 Hz/0.9 Hz structures under the Northridge earthquake excitation are shown in Fig. 13.

It can be seen in Fig. 13 that all resilience loops have the shape of spindle, and under the control of SAEC-PTMD, the area of the structural resilience loop is the smallest. The comparisons of the input energy E_I, dissipated energy by PTMD/SAEC-PTMD E_S, and primary structural hysteretic energy E_H under the Northridge earthquake excitation are presented in Table 8.

It is shown in Table 8 that the input energy of the primary structure with an SAEC-PTMD is the smallest for both the 1.0 Hz and 0.9 Hz structures; however, the energy dissipation ratio E_S/E_I of the SAEC-PTMD is greater than that of the PTMD for both the 1.0 Hz and 0.9 Hz structures, which further illustrates the better control effect and energy dissipation capacity of the SAEC-PTMD. Meanwhile, the hysteretic energy of the primary structure with an SAEC-PTMD is the smallest for both the 1.0 Hz and 0.9 Hz structures, and the hysteretic energy dissipation ratio E_H/E_I

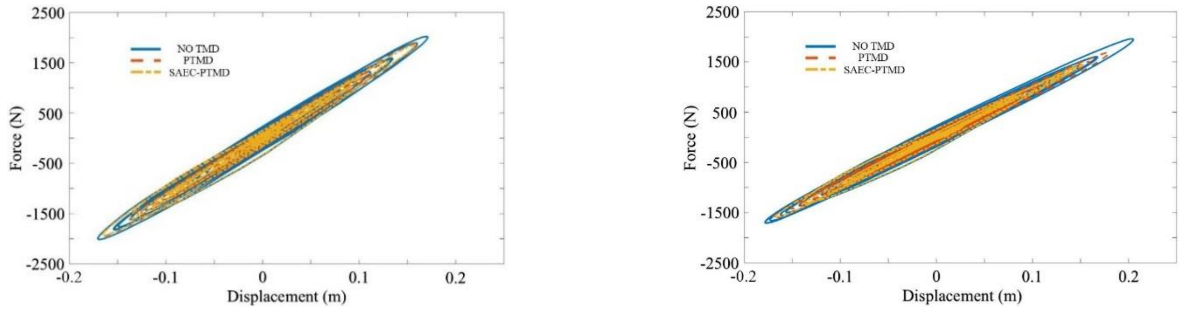

(a) Force/displacement relationship of 1.0 Hz structure

(b) Force/displacement relationship of 0.9 Hz structure

Fig. 13 Comparisons of resilience loops under Northridge ground motion of the nonlinear structure

Table 8 Performance assessment for earthquake energy dissipation of the nonlinear structure

Northridge	1.0 Hz structure			0.9 Hz structure		
	No TMD	PTMD	SAEC-PTMD	PTMD	No TMD	SAEC-PTMD
E_I (J)	1814.99	1619.18	1521.94	1790.06	1654.03	1480.54
E_S (J)		142.27	135.86		95.24	119.77
E_H (J)	563.64	331.88	276.34	550393	365.57	203.10
E_S/E_I (%)		8.79	8.93		5.76	8.09
E_H/E_I (%)	31.05	20.50	18.16	30.78	22.10	13.72

is also the smallest for both the 1.0 Hz and 0.9 Hz structures, which means that SAEC-PTMD can control the development of structural plasticity effectively and protect the safety of primary structure.

7. Conclusions

A novel TMD, the so-called SAEC-PTMD was proposed in this study for protecting civil structures over their full life cycle, which could retune its frequency and damping ratio in real-time. The pendulum of the SAEC-PTMD is adjusted through an HHT-based control algorithm, and the semi-active eddy current damping is adjusted by adjusting the air gap between permanent magnets and conductive plates, based on the LQG-based control algorithm. The vibration control effect of the SAEC-PTMD was studied through numerical simulations under harmonic excitations and four earthquake excitations, for both SDOF linear primary structure and nonlinear primary structure based on the Bouc-Wen model. An optimal passive TMD was used for the comparison, and the detuning effect, which resulted from cumulative damage to the primary structure, was considered.

The mechanisms of the SAEC-PTMD and the combined HHT-LQG algorithm were introduced in detail, and the air gap that would influence the eddy current damping was discussed in detail. According to a series of numerical simulations, the following conclusions were drawn:

- In the case study, the maximum and RMS values of structural acceleration and displacement time history response, structural acceleration, and displacement response spectra were used as evaluation indices. The results indicated that the SAEC-PTMD performed better than the optimal passive TMD, both before and after the cumulative damage to primary structure for all of the abovementioned evaluation indices.
- Power analyses for one earthquake excitation were proposed as an example to further study the energy dissipation capacity of SAEC-PTMDs. It was found that the SAEC-PTMD has a better energy dissipation capacity than the optimal passive TMD.
- In strong earthquakes, the primary structures could enter the nonlinear state. The nonlinear primary structure was simulated based on the Bouc-Wen model. It was found that the SAEC-PTMD still has an excellent vibration control effect and can control the development of structural plasticity effectively and protect the safety of primary structure.
- This study is focused on the concept of the SAEC-PTMD, and its control effect is verified through numerical simulations. In further studies, the model of SAEC-PTMD will be built, and a shaking table test will be proposed to verify its feasibility and control effect.
- Considering the proposed LQG variable damping control algorithm is mainly focused on a linear system, to obtain a better control effect, it is meaningful to propose a novel control algorithm which focuses on the earthquake protection of a nonlinear system in further studies.

Acknowledgments

The authors are grateful for the financial support received from the National Natural Science Foundation of China (Grant no. 51878502).

References

Casciati, F. and Ubertini, F. (2008), “Nonlinear vibration of shallow cables with semiactive tuned mass damper”, *Nonlinear Dyn.*, **53**, 89-106. https://doi.org/10.1007/s11071-007-9298-y

Chung, L., Wu, L., Lien, K., Chen, H. and Huang, H. (2013), “Optimal design of friction pendulum tuned mass damper with varying friction coefficient”, *Struct. Contr. Health Monit.*, **20**, 544-559. https://doi.org/10.1002/stc.514

Contreras, M., Pasala, D. and Nagarajaiah, S. (2014), “Adaptive length SMA pendulum smart tuned mass damper performance in the presence of real time primary system stiffness change”, *Smart Struct. Syst., Int. J.*, **13**(2), 219-233. https://doi.org/10.12989/sss.2014.13.2.219

Den Hartog, J.P. (1985), *Mechanical Vibrations*; McGraw-Hill/Dover: New York, NY, USA.

Dinh, V., Biswajit. B. and Nagarajaiah, S. (2016), “Semi-active control of vibrations of spar type floating offshore wind turbines”, *Smart Struct. Syst., Int. J.*, **18**(4), 683-705. https://doi.org/10.12989/sss.2016.18.4.683

Domizio, M., Ambrosini, D. and Curadelli, O. (2015), “Performance of TMDs on nonlinear structures subjected to near-fault earthquakes”, *Smart Struct. Syst., Int. J.*, **16**(4), 725-742. https://doi.org/10.12989/sss.2015.16.4.725

Eason, R., Sun, C., Dick, A. and Nagarajaiah, S. (2013), “Attenuation of a linear oscillator using a nonlinear and a semi-active tuned mass damper in series”, *J. Sound Vib.*, **332**, 154-166. https://doi.org/10.1016/j.jsv.2012.07.048

Emiliano, M. and Alessandro, D. (2009), “Robust design of mass-uncertain rolling-pendulum TMDs for the seismic protection of buildings”, *Mech. Syst. Signal Pr.*, **23**, 127-147. https://doi.org/10.1016/j.ymssp.2007.08.012

Lin, G., Lin, C., Chen, B. and Soong, T. (2015), “Vibration control performance of tuned mass dampers with resettable variable stiffness”, *Eng. Struct.*, **83**, 187-197. https://doi.org/10.1016/j.engstruct.2014.10.041

Lu, X., Zhang, Q., Weng, D., Zhou, Z., Wang, S., Mahin, S.A., Ding, S. and Qian, F. (2017), “Improving performance of a super tall building using a new eddy-current tuned mass damper”, *Struct. Contr. Health Monit.*, **24**, e1864. https://doi.org/10.1002/stc.1882

Lu, Z., Huang, B., Zhang, Q. and Lu, X. (2018), “Experimental and analytical study on vibration control effects of eddy-current tuned mass dampers under seismic excitations”, *J. Sound Vib.*, **421**, 153-165. https://doi.org/10.1016/j.jsv.2017.10.035

Maiti, S., Bandyopadhyay, R. and Chatterjee, A. (2018), “Vibrations of an Euler-Bernoulli beam with hysteretic damping arising from dispersed frictional microcracks”, *J. Sound Vib.*, **412**, 287-308. https://doi.org/10.1016/j.jsv.2017.09.025

Nagarajaiah, S. (2009), “Adaptive passive, semi-active, smart tuned mass dampers: identification and control using empirical mode decomposition, Hilbert transform, and short-term Fourier transform”, *Struct. Contr. Health Monit*., **16**(7-8), 800-841. https://doi.org/10.1002/stc.349

Nagarajaiah, S. and Sonmez, E. (2007), “Structures with semiactive variable stiffness single/multiple tuned mass dampers”, *J. Struct. Eng.*, **133**(1), 67-77. https://doi.org/10.1061/(ASCE)0733-9445(2007)133:1(67)

Nagarajaiah, S. and Varadarajan, N. (2005), “Short time Fourier transform algorithm for wind response control of buildings with variable stiffness TMD”, *Eng. Struct.*, **27**, 431-441. https://doi.org/10.1016/j.engstruct.2004.10.015

Pasala, D. and Nagarajaiah, S. (2014), “Adaptive-length pendulum smart tuned mass damper using shape-memory-alloy wire for tuning period in real time”, *Smart Struct. Syst., Int. J.*, **13**(2), 203-217. https://doi.org/10.12989/sss.2014.13.2.203

Ramezani, M., Bathaei, A. and Zahrai, S. (2017), “Designing fuzzy systems for optimal parameters of TMDs to reduce seismic response of tall buildings”, *Smart Struct. Syst., Int. J.*, **20**(1), 61-74. https://doi.org/10.12989/sss.2017.20.1.061

Roffel, A., Lourenco, R., Narasimhan, S. and Yarusevych, S. (2011), “Adaptive compensation for detuning in pendulum tuned mass dampers”, *J. Struct. Eng.*, **137**(2), 242-251. https://doi.org/10.1061/(ASCE)ST.1943-541X.0000286

Shi, W., Shan, J. and Lu, X. (2012), “Modal identification of Shanghai world financial center both from free and ambient vibration response”, *Eng. Struct.*, **36**, 14-26. https://doi.org/10.1016/j.engstruct.2011.11.025

Shi, W., Wang, L. and Lu, Z. (2018a), “Study on self-adjustable tuned mass damper with variable mass”, *Struct. Contr. Health Monit*., **25**(3), e2114. https://doi.org/10.1002/stc.2114

Shi, W., Wang, L., Lu, Z. and Gao, H. (2018b), “Study on adaptive-passive and semi-active eddy current tuned mass damper with variable damping”, *Sustain.*, **10**, 99. https://doi.org/10.3390/su10010099

Spencer, B. and Nagarajaiah, S. (2003), “State of the art of structural control”, *J. Struct. Eng*., **129**(7), 845-856. https://doi.org/10.1061/(ASCE)0733-9445(2003)129:7(845)

Sun, C. (2018), “Semi-active control of monopile offshore wind turbines under multi-hazards”, *Mech. Syst. Signal Pr.*, **99**, 285-305. https://doi.org/10.1016/j.ymssp.2017.06.016

Sun, C. and Nagarajaiah, S. (2014), “Study on semi-active tuned mass damper with variable damping and stiffness under seismic excitations”, *Struct. Contr. Health Monit.*, **21**(6), 890-906. https://doi.org/10.1002/stc.1620

Sun, C., Eason, R., Nagarajaiah, S. and Dick, A. (2013), “Hardening Düffing oscillator attenuation using a nonlinear TMD, a semi-active TMD and multiple TMD”, *J. Sound Vib.*, **332**, 674-686. https://doi.org/10.1016/j.jsv.2012.10.016

Varadarajan, N. and Nagarajaiah, S. (2004), “Wind response control of building with variable stiffness tuned mass damper using empirical mode decomposition/Hilbert transform”, *J. Eng. Mech.*, **130**(4), 451-458. https://doi.org/10.1061/(ASCE)0733-9399(2004)130:4(451)

Wang, J. and Lin, C. (2015), “Extracting parameters of TMD and primary structure from the combined system responses”, *Smart Struct. Syst., Int. J.*, **16**(5), 937-960. https://doi.org/10.12989/sss.2015.16.5.937

Wang, Z., Chen, Z. and Wang, J. (2012), “Feasibility study of a large-scale tuned mass damper with eddy current damping mechanism”, *Earthq. Eng. Eng. Vib.*, **11**, 391-401. https://doi.org/10.1007/s11803-012-0129-x

Wang, L., Shi, W. and Zhou, Y. (2018), “Study on self-adjustable variable pendulum tuned mass damper”, *Struct. Des. Tall Special Build.*, **28**(1), e1561. https://doi.org/10.1002/tal.1561

Wang, L., Shi, W., Li, X., Zhang, Q. and Zhou, Y. (2019), “An adaptive-passive retuning device for a pendulum tuned mass damper considering mass uncertainty and optimum frequency”, *Struct Control Health Monit.*, **26**(7), e2377. https://doi.org/10.1002/stc.2377

Waubke, H. and Kasess, C. (2017), “Gaussian closure technique for chain like structures with elasto-plastic elements described by the Bouc hysteresis”, *J. Sound Vib.*, **408**, 73-86. https://doi.org/10.1016/j.jsv.2017.07.020

BS